Check for updates

A Drill Pipe-Embedded Vibration Energy Harvester and Self-Powered Sensor Based on Annular Type Triboelectric Nanogenerator for Measurement while Drilling System

Taili Du, Fangyang Dong, Ruijiang Xu, Yongjiu Zou, Hao Wang, Xingjia Jiang, Ziyue Xi, Haichao Yuan, Yuewen Zhang,* Peiting Sun,* and Minyi Xu*

Measurement while drilling (MWD) system of offshore drill pipe is of great significance for safety production. It is greatly demanded to develop a sustainable power supply as well as self-powered sensors for the MWD system. In this work, a drill pipe-embedded annular type triboelectric nanogenerator (AT-TENG) is proposed and systematically investigated, and it consists of an annular silicone rubber and a pair of electrodes. The design of the AT-TENG allows the silicone rubber to contact and separate with the electrodes easily in a narrow space under arbitrary direction vibration to realize power generation. The experimental results show that the peak power density of AT-TENG with single-pair electrode reaches 63.7 W m^{-3} under the vibration frequency of 4 Hz and amplitude of 100 mm. The minimum peak voltage is >65 V within 360° lateral vibration range. The peak voltage achieves 351.62 V under the third-order natural frequency. In addition, the amplitude and frequency obtained from the voltage signals exhibit linearly with those of actual vibration. The mean error between the frequency detected by AT-TENG and actual frequency is <0.03%. Thus, the AT-TENG can serve as an energy harvester and self-powered vibration sensor.

1. Introduction

Nowadays, offshore platform plays a vital role in modern offshore oil exploitation, while the drilling device is one of the most important equipments on the platform.[1,2] The working condition of drilling drill pipe has a dominant influence on the

T. Du, F. Dong, R. Xu, Y. Zou, H. Wang, X. Jiang, Z. Xi, H. Yuan, M. Xu
Dalian Key Laboratory of Marine Micro/Nano Energy
and Self-powered Systems
Marine Engineering College
Dalian Maritime University
Dalian 116026, China
E-mail: xuminyi@dlmu.edu.cn
T. Du, Y. Zou, X. Jiang, Y. Zhang, P. Sun
Collaborative Innovation Research Institute of Autonomous Ship
Dalian Maritime University
Dalian 116026, China
E-mail: zhangyuewen@dlmu.edu.cn; sunptg@dlmu.edu.cn
T. Du, Y. Zou, X. Jiang, Y. Zhang, P. Sun
Marine Engineering College
Dalian Maritime University
Dalian 116026, China

whole drilling process. Monitoring the working condition of the drilling device is mainly carried out by the measurement while drilling (MWD) system or logging while drilling (LWD) system.[3,4] Further, available measurement tools in the market can achieve the sensing functions of the drill pipe, including RMS, peak and average vibration etc., which have been shown to alleviate overall drilling challenges. However, at present, the power source of the MWD system mainly includes cable power supply,[5] battery power supply,[6] and turbine generator,[7] which provide certain guarantee for the working condition monitoring of drilling device. However, due to the long length of the drill pipe, on one hand, the cable power supply increases the construction difficulty and construction cost, and on the other hand, the vibration generated during the drilling process may damage the cable. If battery is adopted to supply power, there are problems such as short battery life, low operation efficiency because of battery replacement, and high maintenance cost.[8,9] Moreover, the battery's post-treatment process can lead to further environmental detriment. Although the turbine generators offer significant advantages over battery power in terms of quantity of power and sustainability, they also have the disadvantages of complex construction, high cost, and stringent requirements of flow and viscosity.[7,10] Meanwhile, the drill pipe inevitably produces vibration, especially lateral vibration, during operation,[11–14] while the vibrational energy is widely distributed throughout the whole drill pipe assembly, but is underutilized. Therefore, it is a good choice to develop a new approach to utilize the vibration energy, which cannot only power the MWD system, but also realize the self-powered monitoring of the drill pipe.

The triboelectric nanogenerator (TENG) was invented by Wang etc. in 2012.[15] Combining contact electrification and electrostatic induction,[16,17] the TENG provides a new solution to achieve those functions. Even more, the TENG features low cost, easy fabrication, wide range choice of materials, and high conversion efficiency, especially for randomly distributed, irregular and low frequency energy.[18–20] In recent years, energy harvesting devices and self-powered sensing systems based TENG technology have attracted more and more attention with

**ADVANCED
SCIENCE NEWS**
www.advancedsciencenews.com

**ADVANCED
MATERIALS
TECHNOLOGIES**
www.advmattechnol.de

the increasing demand of the huge number of wireless nodes in various fields. In different fields, researchers have applied TENGs to collect different environmental energies such as mechanical vibration energy,[21–23] wind energy,[24,25] ocean current energy[26] and wave energy,[27] and realized self-powered sensing of vibration,[28,29] wind speed,[30] gas and liquid flow velocity,[31] tactile,[32] tilting angle[33] and gas composition[34] based on TENG technology. In the field of drilling, a series of studies have been carried out in the areas of down hole vibration and rotation[35,36] energy collection, and self-powered vibration monitoring.[37] However, the installation of these devices will inevitably affect the normal operation of the drill pipe, because they are arranged outside of the drill pipe. This is also detrimental to the need for distributed power supply and distributed sensing along hundreds of meters of drill pipe, thus impeding the development of intelligent drill pipe.

Therefore, the present work proposes a novel drill-pipe embedded annular type triboelectric nanogenerator (AT-TENG) to realize the vibration energy harvesting and self-powered vibration sensing of the offshore drill pipe. By placing AT-TENG in the annular space dug out in the wear-resistant ring, on one hand, it does not affect the normal operation of the drill pipe. And it can be protected by the outside of the wear-resistant ring of the drill pipe, which reduces the impact of the wear and collision during the drilling process and ensures its working performance in actual working conditions to the maximum extent. It is capable of converting the vibration energy into electricity as long as the drill pipe vibrates. According to the experimental results, the open-circuit voltage (V_{OC}), short-circuit current (I_{sc}) of AT-TENG can reach 334.75 V and 6.24 µA respectively with the vibration frequency of 4 Hz and amplitude of 100 mm. The peak power density reaches 63.7 W m^{-3} while the external matching resistance is 400 MΩ. Moreover, it can light up more than 100 LEDs and power a commercial temperature and humidity sensor. Furthermore, AT-TENG also yields desirable performance at the first-, second-, and third-order natural frequencies according to the test results. Besides being a vibration energy harvester, the AT-TENG is found to generate an output voltage exhibiting a good linear correlation with vibration amplitude and frequency making it a promising self-powered vibration sensor for the drill pipe.

2. Results and Discussion

2.1. Structure and Working Principle of AT-TENG

The actual arrangement of the drill pipe is fully considered to optimize the design of the AT-TENG, so that the AT-TENG can accommodate the application scenario preferably and minimize the impact on the actual production process. Generally, the length of the drill pipe assembly mainly depends on the water depth and the distance between the oil reserves and the seabed, which can reach several hundreds or even thousands of meters. Hence, the drill pipe assembly is composed of a lot of standard drill pipes, which are connected together through threaded or other connections.

The axial section across the centerline of the drill pipe is shown in Figure S1 (Supporting Information). The drill pipe is composed of pin end, box end, and main part. In order to secure the reliability of the drilling process, protruding structures with an outer diameter greater than that of the main drill pipe in both pin end and box end are fabricated to withstand the vibration impact of the drill pipe. This section of protruding structure can be regarded as wear-resistant ring as well.

The AT-TENG is designed and fabricated to be placed in the annular space dug out in the protruding section according to the actual layout of the drill pipe. As thus, this arrangement changes the original layout of the drill pipe to the minimum extent, which is one of the highlights of the AT-TENG in this work. Moreover, this design can reduce the influence on the normal working of the drill pipe to the maximum extent, because the AT-TENG can be protected by the outer part of the wear-resistant ring, and it is easier to take measures to keep the tight of the dugout annular space.

Due to its unique design, the AT-TENG is mainly applied in the offshore drill pipe to convert the vibration energy to electricity, and the application scenario is shown in **Figure 1**a. Figure 1b shows the layout of the AT-TENG embedded in the drill pipe. Each wear-resistant ring can be equipped with one AT-TENG, which realizes the distributed power supply of the MWD system. Further, it can reduce the external impact from the drill pipe length and keep comprehensive monitoring of the overall drill pipe. The AT-TENG is designed and fabricated according to the actual dimension of the drill pipe, so as to verify its actual output performance. The shell of the AT-TENG consists of two acrylic tubes with the inner diameter of 120 mm for the external tube, and the outer diameter of 100 mm for the internal tube, both of which are 5 mm thick. Consequently, the clearance between the two acrylic tubes is 10 mm, which is adapted to the annular space dug out in the wear-resistant ring. Then, the silicone rubber ring is placed in the annular space to be one of the tribo-materials. The copper film is attached to both sides of the clearance to be the other tribo-material and the electrodes as well, which is shown in Figure 1c and the top view image of the AT-TENG is illustrated in Figure 1d.

The working principle of the AT-TENG is demonstrated in Figure 1e. As shown in Figure 1e(i), in the initial state, the silicone rubber ring contacts with one electrode. After the silicone rubber ring contacts with the copper film for a few times, negative charges is accumulated on the surface of the silicone rubber ring due to the electronegativity of it compared with that of the copper film. At the same time, there is equal positive charge on the copper film to achieve electric potential equilibrium. With the vibration of the drill pipe, the silicone rubber ring separates from the initial copper electrode and moves to the other one, which breaks the electric potential balance. As the silicone rubber ring moves away from the initial copper film, electrons flows between the two electrodes, so current is generated in the external circuit to balance the electric potential difference, as shown in Figure 1e(ii). While the silicone rubber ring contacts with the opposite copper electrode, new potential equilibrium is achieved, and the transfer of electrons between the two electrodes stops, as demonstrated in Figure 1e(iii). As the drill pipe vibrates continuously, the silicone rubber ring moves in the opposite direction, which is illustrated in Figure 1e(iv). Meanwhile, the imbalance of electric potential leads to the movement of electrons in the opposite direction between two copper electrodes, resulting in
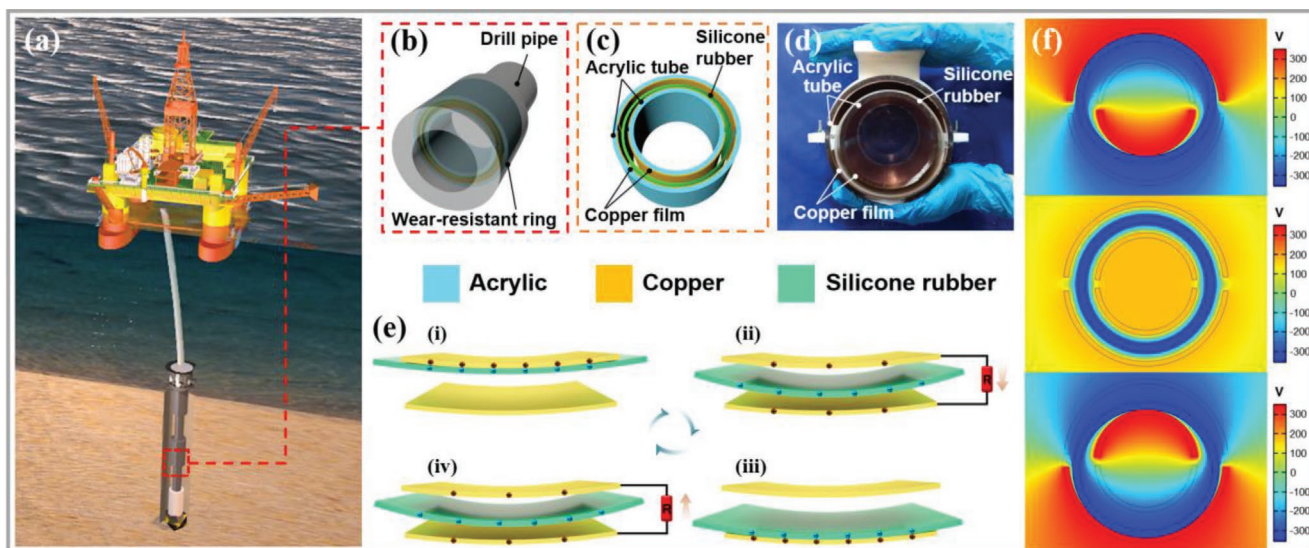
Figure 1. Application scenario, structure, and working principle of the AT-TENG. a) Schematic of the AT-TENG applied to the drill pipe; b) arrangement position of the AT-TENG embedded in the drill pipe; c) structure schematic and d) top view image of the AT-TENG; e) working principle of the AT-TENG; f) the qualitative electric potential distribution simulation results of the AT-TENG by COMSOL Multiphysics.

contrary current in the external circuit. As a result, alternating current is generated during the continuous contact and separation process between two copper electrodes and the silicone rubber ring to convert the vibration energy into electrical energy.

From the above analysis, it is obvious that the AT-TENG can be essentially regarded as the freestanding mode TENG.[17] And, according to the theory of the freestanding mode TENG,[38] the governing equation of it can be written as:

$$V = -\frac{1}{C}Q + V_{OC} = -\frac{d_0 + g}{\varepsilon_0 S}Q + \frac{2\sigma x}{\varepsilon_0} \tag{1}$$

where, V represents the voltage of the AT-TENG, C is the capacitance, Q means the transferred charge, d_0 and g are the effective dielectric thickness and total air gap between two copper electrodes, ε_0 is the dielectric constant in vacuum, S means the effective contact area, σ represents the charge density on the silicone rubber ring, and x is the distance between the silicone rubber ring and the copper electrode.

Moreover, the qualitative electric potential simulation is conducted by COMSOL Multiphysics to verify the practicability of the working principle before launching the experiment. As depicted in Figure 1f, the electric potential distribution and variation trend are consistent with the theoretical analysis, which supports the working principle analysis in terms of simulation.

### 2.2. Output Performance of AT-TENG

To test the output performance of AT-TENG and study the working status of the silicone rubber ring, a test system of the AT-TENG has been built. As shown in **Figure 2**a, the test system is composed of servo drive, linear motor, data acquisition unit, Keithley 6514 electrometer, data recorder (based on LabView), high-speed camera and so on. For achieving larger contact area between the silicone rubber and copper electrode

to enhance the output performance of the AT-TENG, two pairs of the electrodes are designed as shown in Figure 1c. The output current of the AT-TENG with double-pair electrodes under different vibration frequencies of 1, 2, 3, and 4 Hz and fixed amplitude of 100 mm is much higher than that of the AT-TENG with single-pair electrode, which is exhibited in Figure 2b. The output voltage, transferred charges of the AT-TENG with double-pair and single-pair electrodes are exhibited in Figure S2 (Supporting Information), which also show the similar result as the above output current comparison between AT-TENG with double- and single-pair electrodes. Therefore, the AT-TENG with single-pair electrode is discussed in this work, so as to show the output performance of the AT-TENG more conveniently and intuitively. Since the AT-TENG is embedded in the wear resistant ring, its movement is mainly motivated by the vibration of the drill pipe, and the kinetic energy can be expressed as follows:[39]

$$E = \frac{1}{2}m\int_0^L \left(\left(\frac{\partial u}{\partial t}\right)^2 + \left(\frac{\partial v}{\partial t}\right)^2\right)dx \tag{2}$$

where, E is the kinetic energy of the drill pipe, m is the mass of the drill pipe, L is the length of the drill pipe, u is the axial displacement of the drill pipe, and v is the transverse displacement of the drill pipe, respectively.

According to that, the vibration frequency and amplitude of the drill pipe are two key factors that affect the movement and output performance of AT-TENG. Hence, the influence of different exciting vibration frequencies, amplitudes on AT-TENG output performance is explored. Besides, the thickness of the silicone rubber ring also affects its movement, so different silicone rubber rings with different thickness are fabricated and tested under lateral vibration. Moreover, for different frequency and amplitude of the drill pipe, the silicone rubber ring thickness with highest output may be different, but the results show
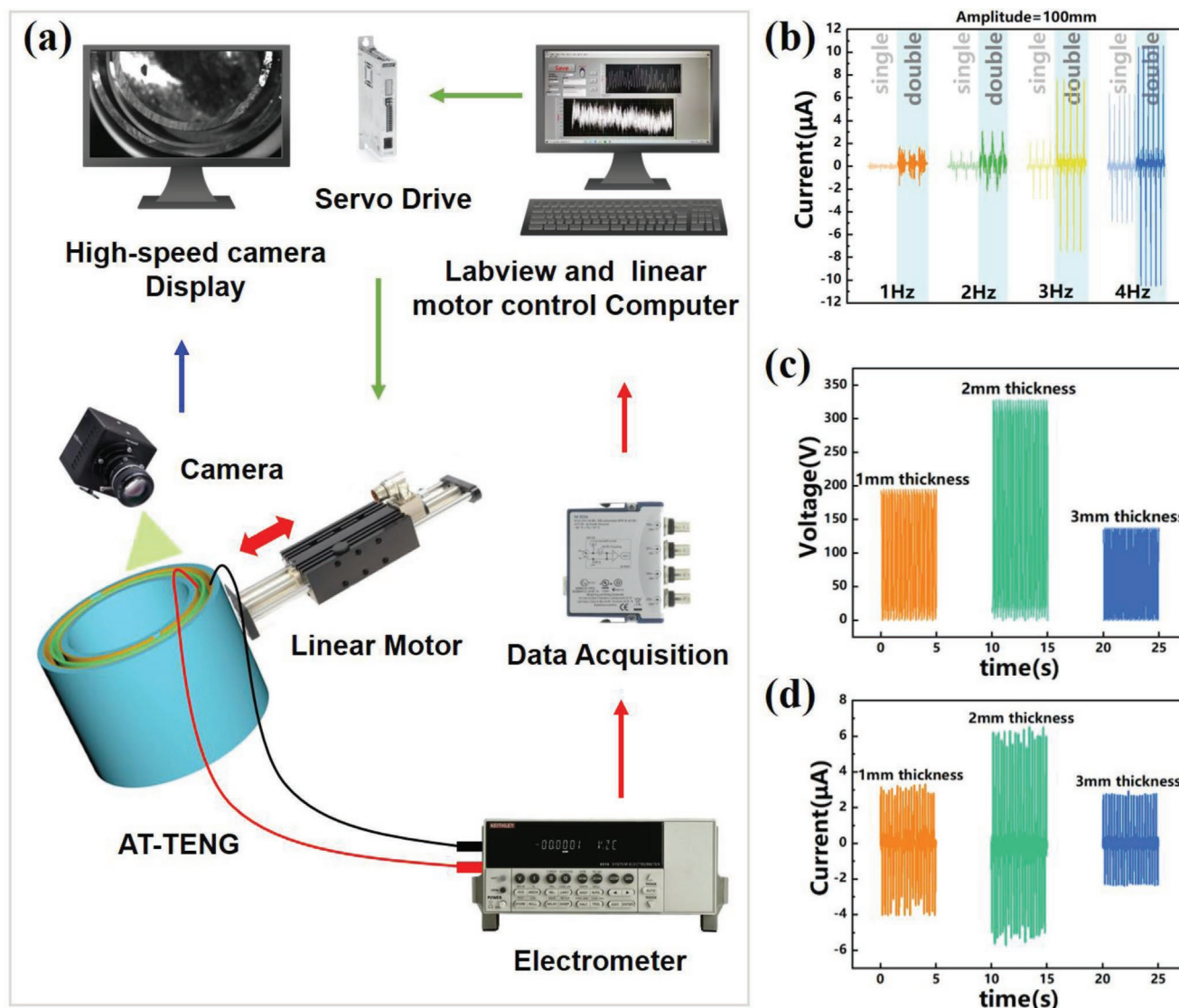
Figure 2. Test system for AT-TENG. a) Test apparatuses and test flowchart for AT-TENG; b) short-circuit current comparison between AT-TENGs with double-pair and single-pair electrodes; c) open-circuit voltage and d) short-circuit current comparison among AT-TENGs with silicone rubber ring thickness of 1, 2, and 3 mm.

that the AT-TENG with the silicone rubber ring of 2 mm thickness has the highest output. As illustrated in Figure 2c,d, the peak voltage of the AT-TENG with different silicone rubber ring thickness of 1, 2, and 3 mm are 195, 334.75, and 137.7 V, and the peak currents are 4, 6.24, and 2.76 µA, respectively. Furthermore, the output performance of the AT-TENG with different silicone rubber ring thickness is tested under vibration conditions of different vibration frequency and amplitude, which is shown in Figure S3 (Supporting Information). It is mainly because that the silicone rubber ring with thickness of 1 mm in the design of this work is relatively lighter, the contact between the electrode and it is insufficient due to the distortion under the vibration excitation, so its output performance is lower in consequence. As for the silicone rubber ring with thickness of 3 mm, its deformation is low due to its thicker thickness, which limits its contact area with the electrode, so its output performance is also lower than that of the 2 mm one. On account

of above analysis, the AT-TENG with 2 mm thickness silicone rubber ring is determined to be the final object of this study.

By referring to research,[40,41] the first-, second-, and third-order natural frequencies of the drill pipe are 1.25, 2.93, and 4.18 Hz, and the vibration energy under the natural frequencies is larger than that under other frequencies, so the frequency range of 1—5 Hz (with a step of 1 Hz) is adopted in this work. In addition, the maximum vibration amplitude of the drill pipe is limited <100 mm,[42] so the vibration amplitude range of 10—100 mm with the interval of every 10 mm is employed. The output voltage of the AT-TENG varies with the vibration frequency of the drill pipe is illustrated in **Figure 3**a. The voltage basically increases with the increase of the frequency linearly within 2—5 Hz, and the linear correlation coefficient is 0.9801. Figure 3b,c demonstrates that the current and the transferred charge increases with the increase of frequency as well, the linear correlation coefficients of which are 0.9543 and 0.9893,
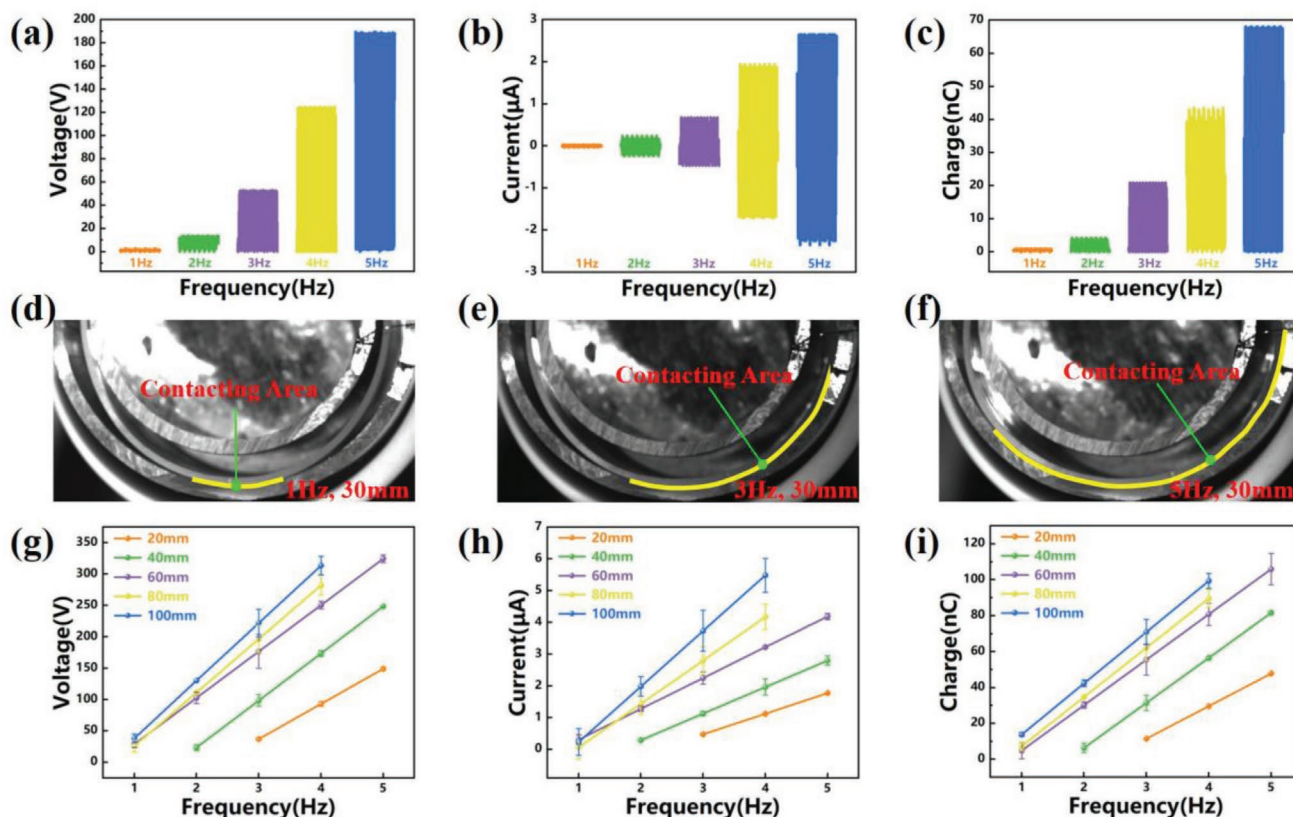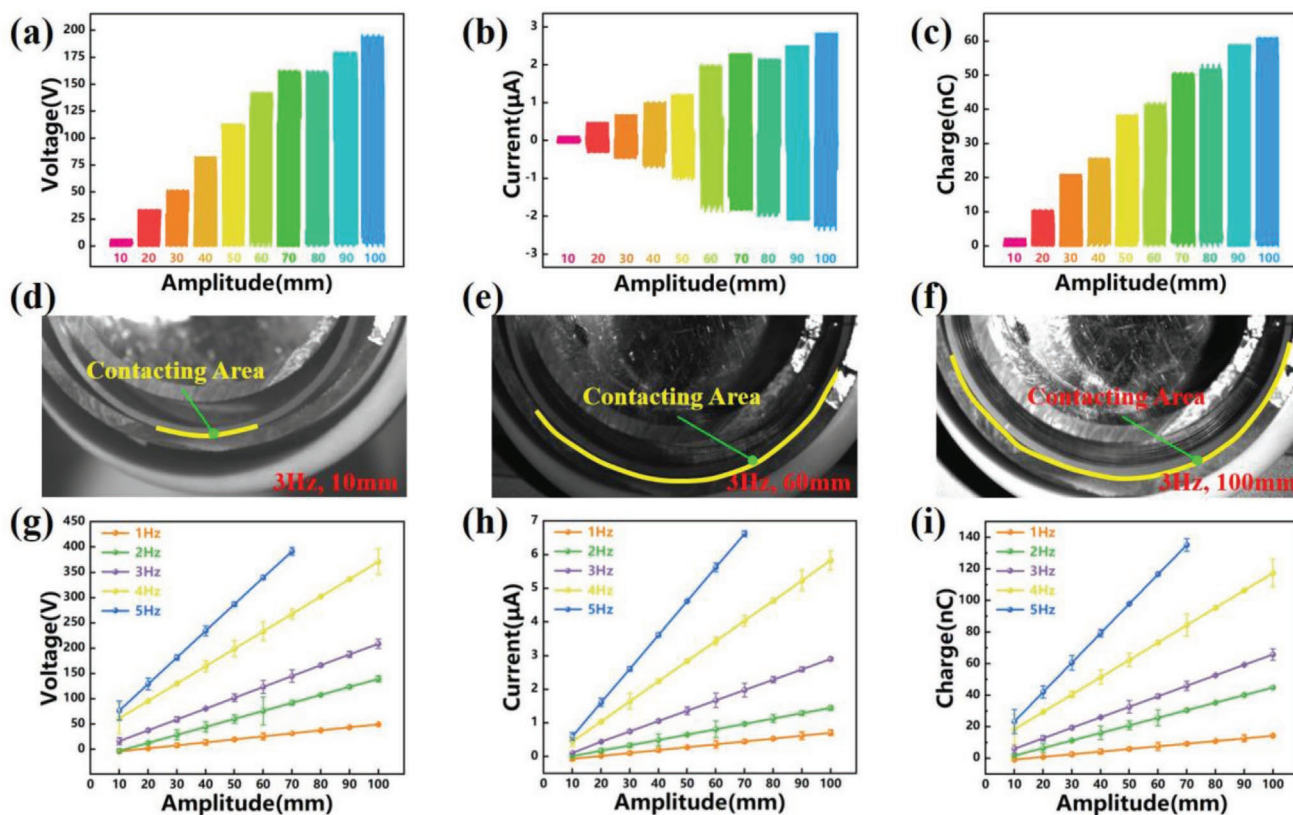
Figure 3. Output performance of the AT-TENG under different frequencies with different fixed vibration amplitudes. a) Open-circuit voltage, b) short-circuit current, and c) transferred charges of the AT-TENG under different frequencies with the fixed amplitude of 30 mm. Silicone rubber ring working status at vibration frequency of d) 1, e) 3, and f) 5 Hz with the amplitude of 30 mm. g) Open-circuit voltage, h) short-circuit current, and i) transferred charges of the AT-TENG under different frequencies with the fixed amplitudes of 20, 40, 60, 80, and 100 mm.

respectively. The main reason for this trend is that the silicone rubber ring obtains more energy with the increase of the frequency at constant amplitude, leading to the increase of the contact area between the silicone rubber and the electrode, thus enhancing the output performance.

The working status of the AT-TENG under frequencies of 1, 3, 5 Hz and amplitude of 30 mm, which is filmed by the high-speed camera, is shown in Figure 3d–f. In addition, the moving status of the silicone rubber ring in the AT-TENG under different frequencies with fixed amplitude of 30 mm is demonstrated in Video S1 (Supporting Information). The contact area under external excitation with increasing frequency from 1 to 5 Hz increases gradually. Furthermore, it follows that the silicone rubber ring in the AT-TENG under the vibration of 1 Hz shows smaller motion because of the smaller kinetic energy, which is not adequate to motivate the contact-separation between the silicone rubber ring and the electrode according to the Equation (2). Moreover, the times of the contact-separation cycle between the silicone rubber ring and one electrode is equal to that of the external vibration cycle under the vibration frequency of 3 and 5 Hz. Under the effects of the contacting area and number of contacts, the output performance improves with the increasing frequency under fixed amplitude. The main reason for this phenomenon is that the kinetic energy of the external excitation is larger with larger frequency and fixed amplitude.

The variations of voltage, current and transferred charge of AT-TENG with frequency under different fixed amplitudes are shown in Figure 3g–i. It is observed that the voltage, the current, and the transferred charge increase with frequency. Especially, the relationships between the voltage, transferred charge, and the frequency are almost linear and hardly overlap among different amplitudes. In view of this characteristics, the AT-TENG can also be used as a self-powered vibration frequency sensor. However, what needs to be pointed out is that the output performance test under the condition of 5 Hz with amplitudes above 80 mm cannot be achieved due to the capacity limitation of the linear motor. Therefore, the output performance of the AT-TENG with the amplitudes of 80, 90, and 100 mm are only carried out under the frequency range of 1—4 Hz. Furthermore, the output performance of the AT-TENG at low frequency and low amplitude, including the voltage, current and transferred charge, does not conform to the linear relationship to some extent. The reason for this phenomenon is that the energy obtained by the silicone rubber ring is not enough to make it fully and regularly contact with the copper electrode under the condition of such low vibration. Even though, AT-TENG still has a certain output power, which reflects its low frequency adaptability from some aspects.

To study the output performance of the AT-TENG under different vibration conditions in more detail, the variation of the

**ADVANCED
SCIENCE NEWS**
www.advancedsciencenews.com

**ADVANCED
MATERIALS
TECHNOLOGIES**
www.advmattechnol.de

Figure 4. Output performance of the AT-TENG under different amplitudes with different fixed vibration frequencies. a) Open-circuit voltage, b) short-circuit current, and c) transferred charges of the AT-TENG under different frequencies with the fixed vibration frequency of 3 Hz. Silicone rubber ring working status at vibration amplitude of d) 10, e) 60, and f) 100 mm with the vibration frequency of 3 Hz. g) Open-circuit voltage, h) short-circuit current, and i) transferred charges of the AT-TENG under different amplitudes with the fixed vibration frequencies of 1, 2, 3, 4, and 5 Hz.

AT-TENG's output performance with amplitude under different frequencies is carried out. The variation of the voltage with different amplitude under the vibration frequency of 3 Hz is exhibited in **Figure 4**a, in which it can be seen that the voltage rises with an increase of the vibration amplitude. Moreover, the linear correlation coefficient turns out to be 0.9644, showing excellent linear relationship between the voltage and amplitude. In addition, the current and transferred charge have the homologous trend with the amplitude shown in Figure 4b,c. The linear correlation coefficients reach 0.9647 and 0.9682, respectively after the correlation analysis. The results are in accordance with the above analysis due to an increase of the kinetic energy obtained by the AT-TENG.

Figure 4d–f shows the contact statuses between the silicone rubber ring and the electrodes with different amplitudes of 10, 60, and 100 mm and frequency fixed at 3 Hz, which are taken by the high-speed camera. As shown in Figure 4d–f and Video S2 (Supporting Information), the contact area between the silicone rubber ring and electrodes increases with the growth of the amplitude under fixed frequency, thereby enlarge the output performance of the AT-TENG.

The relationships between the voltage, the current, the transferred charge, and the amplitude under fixed frequencies of 1—5 Hz, are depicted in Figure 4g–i. The results show the similar trend as that with the frequency of 3 Hz and there is almost no overlap among different vibration frequencies as well.

Especially, because of the characteristics of high open-circuit voltage of the AT-TENG, the peak voltage is the best signal that can be used to represent the amplitude. So, AT-TENG has the potential to be applied on self-powered vibration amplitude sensing in addition to being a self-powered frequency sensor.

2.3. Demonstration of the AT-TENG

Based on the above test results, the relationship among the voltage, the vibration amplitude, and the frequency can be obtained, which is demonstrated in **Figure 5**a. The output voltage enhances step by step with the increase of the amplitude and frequency. The open-circuit voltage increases from 0.95 V with the frequency of 1 Hz and amplitude of 10 mm to 334.75 V with the frequency of 4 Hz and amplitude of 100 mm. Additionally, the peak power density generated by the AT-TENG can reach 63.7 W m^{-3} with the matching resistance of 400 MΩ in the external circuit under the frequency of 4 Hz and amplitude of 100 mm, which is illustrated in Figure 5b. Meanwhile, the AT-TENG can light up more than 100 LEDs as shown in the inset of Figure 5b. Furthermore, it is then applied to charge different capacitors. As demonstrated in Figure 5c, the smaller the capacitor, the higher the charge rate. The voltages of the 10, 22, 47, 100, and 220 µF capacitors can achieve 8.3, 4.19, 2.1, 0.87, and 0.45 V respectively after 100 s charging. Then, the
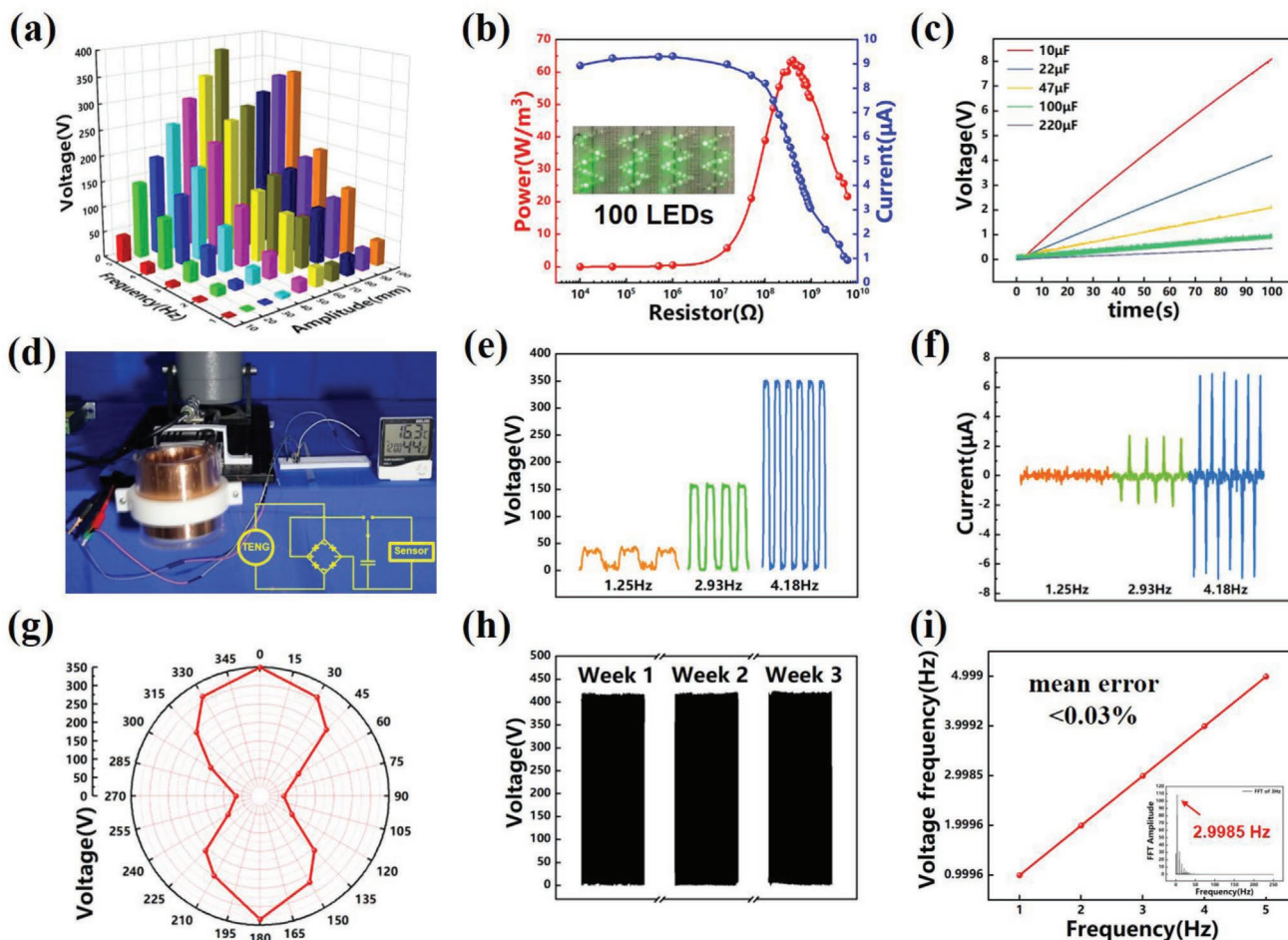
Figure 5. Demonstration of the AT-TENG in power generation. a) Open-circuit voltage of the AT-TENG under different vibration conditions; b) measured output current and calculated output power-resistance profile for AT-TENG; c) voltage curves of different capacitors charged by AT-TENG after rectifying circuit with vibration frequency of 4 Hz and amplitude of 100 mm; d) the illustration of a commercial temperature and humidity sensor powered by AT-TENG; e) open-circuit voltage and f) short-circuit current of AT-TENG under the first-, second-, and third-order natural frequencies and amplitude of 100 mm; g) dependence of the open-circuit voltage of the AT-TENG on the lateral vibration direction; h) durability test result of the AT-TENG within 3 weeks; i) relationship between measured frequency by AT-TENG and actual vibration frequency motivated by linear motor.

power stored in the 100 µF capacitor after continuous charging for 300 s is capable of powering a commercial temperature and humidity sensor, which is demonstrated in Figure 5d and Video S3 (Supporting Information). And the rectifying circuit for powering the sensor is presented in the inset of Figure 5d.

On basis of exploring the power generation performance of AT-TENG under different vibration conditions, the output performance of the AT-TENG under first-, second-, and third-order natural frequencies is studied. The voltage and current under these three natural frequencies and amplitude of 100 mm are shown in Figure 5e,f, the voltage and current of which increase from 43.6 V and 0.6 µA under first-order natural frequency to 351.62 V and 7.02 µA under third-order natural frequency.

Moreover, as shown in Figure 5g, the AT-TENG shows appreciable output performance when the lateral vibration direction changes in any direction, indicating that the vibration energy can be effectively harvested from arbitrary directions. The open-circuit voltage is always above 65 V and the peak voltage is >330 V with the vibration angle of 0° and 180°. In addition, the

vibration of the drill pipe is periodical that may lead to insufficient energy to excite the power generation of AT-TENG. At this time, the power generated by the AT-TENG under adequate vibration excitation can be stored in a storage device, and power the MWDs in the periodical inadequate vibration energy time. Furthermore, as mentioned above, AT-TENG should have the ability to work for long time with the drill pipe, so the durability of it should be brought into consideration. To verify the robustness and durability of AT-TENG, the output performance of it has been tested at random intervals, and keeps stable. In particular, we carry out tests for specific time once every week in 3 weeks continuously, which is shown in Figure 5h, indicating that the output performance of the AT-TENG hardly degrades after 3 weeks, which shows the robustness and durability of it.

The vibration sensing performance is systematically studied in order to verify its potential to be a self-powered vibration sensor. The frequency of 3 Hz is monitored to be 2.9985 Hz after fast Fourier transform (FFT) of open-circuit voltage and displayed on LabView based computer, which is shown in the inset

**ADVANCED
SCIENCE NEWS**
www.advancedsciencenews.com

**ADVANCED
MATERIALS
TECHNOLOGIES**
www.advmattechnol.de

of Figure 5i and Video S4 (Supporting Information). The mean error between actual frequency and frequency measured by the AT-TENG is <0.03% as demonstrated in Figure 5i. Based on the test results, the peak voltage and the FFT result of the output signal of AT-TENG can both be applied to accomplish the vibration sensing function. Therefore, it is proved that the AT-TENG in this work can be adopted as a drill pipe vibration energy harvester and a self-powered vibration frequency sensor as well.

Moreover, the output capability and sensing performance of the AT-TENG are affected by the actual working conditions, including high temperature, high salinity, high humidity, etc., which will be the emphatic aspects for our further study. Nonetheless, due to the unique design of the AT-TENG, it is hardly influenced by the real environment because it is embedded in the drill pipe and isolated from the outside environment. So, it is promising for practical applications of the AT-TENG in the field of offshore drill pipe in future.

3. Conclusions

In summary, this work proposes a novel drill pipe-embedded AT-TENG for vibration energy harvesting and self-powered sensing for the offshore drill pipe. The AT-TENG is particularly designed to be embedded in the dugout annular space of the wear-resistant ring, which hardly affects the normal drilling process. The experimental results show that the open-circuit voltage, the short-circuit current, and the transferred charge of the AT-TENG can reach 334.75 V, 6.24 μA and 105.2 nC, respectively, even with single-pair electrodes (under the vibration frequency of 4 Hz and amplitude of 100 mm). The peak power density achieves 63.7 W m^{-3} with single-pair electrodes, which is able to charge a 10 μF capacitor to 8.3 V in 100 s, light up more than 100 LEDs, and power a commercial temperature and humidity sensor. Further, the output voltage of AT-TENG comes up to 351.62 V under the third-order natural frequency and amplitude of 100 mm, and the output performance barely deteriorates after 3 weeks. Evenmore, the AT-TENG shows desirable energy harvesting performance under arbitrary direction vibration, exhibiting its promising to be a vibration energy harvester for the offshore drill pipe. Additionally, the AT-TENG can also be applied as a self-powered vibration sensor, and the mean error in detecting the vibration frequency is <0.03%. This work can be used extensively in the energy harvesting of offshore drill pipe, and realize the self-powered sensing of drill pipe working conditions, which can improve the condition monitoring and intelligent level of offshore oil drill pipe.

4. Experimental Section

Fabrication of the AT-TENG: One acrylic tube with inner diameter of 120 mm and the other acrylic tube with outer diameter of 100 mm, and both of them with length of 100 mm and wall thickness of 5 mm were cut into two half-cylinders from the centerline by a laser cutting machine respectively. Copper films with thickness of 0.1 mm were pasted on the outside of two smaller half-cylinders, and the inside of the other two half-cylinders. The distances between the copper film edge and the cutting edge of half-cylinders were all 5 mm. The copper wire was adhered to the copper film on four half-cylinders as the signal acquisition wire. Then, four half-cylinders were assembled to the original state before cutting.

A circular acrylic plate with diameter of 135 mm, which was a little larger than the outer diameter of the greater acrylic tube was cut by the laser cutting machine. After assembly, the ends of two acrylic tubes were glued onto the circular acrylic plate, and the centerline of two acrylic tubes was consistent with the center line of the plate, thus forming an annular space. The three silicone rubber rang with different thicknesses by pouring the well-stirred silicone rubber into the prepared molds and then cooling down. Three molds were made of PLA material and printed by a 3D printer. The nominal diameter of the center of three molds was 110 mm uniformly, and its thickness was 1, 2, and 3 mm, respectively. The fabricated silicone rubber rings were washed by the deionized water and alcohol, and then placed into the annular space of the AT-TENG. Additionally, a clamp device was also made by the 3D printer to hold the AT-TENG on the test bench.

Output Performance Measurement of the AT-TENG: The output signals of the AT-TENG were measured by Keithley 6514 electrometer. The vibration excitation is supplied by the test system illustrated in Figure 2a, in which the controlling software on the computer was applied to control the motion of the linear motor (Linmot E1100), such as the vibration frequency and amplitude. The output signal of AT-TENG was acquired by the data acquisition card, delivered to Keithley 6514 electrometer, then displayed and stored in the LabView-based computer.

Statistical Analysis: Data were given as mean ± se. Estimates of statistical significance were performed by Anova (Tukey test, SigmaStat software), values of $p < 0.05$ being considered significant.

Supporting Information

Supporting Information is available from the Wiley Online Library or from the author.

Conflict of Interest

The authors declare no conflict of interest.

Data Availability Statement

The data that support the findings of this study are available in the supplementary material of this article.

[1] U. J. F. Aarsnes, O. M. Aamo, *J. Sound Vib* **2016**, *360*, 239.

[2] B. L. Zhang, Q. L. Han, X. M. Zhang, *Nonlinear Dynam.* **2017**, *89*, 755.

[3] J. van Eldert, H. Schunnesson, D. Saiang, J. Funehag, *Tunn. Undergr. Space Technol.* **2020**, *103*, 103467.

[4] H. Q. Li, R. H. Wang, *Sensors* **2021**, *21*, 24.

[5] C. Zhang, H. B. Dong, J. Ge, H. Liu, *IEEE Access* **2021**, *9*, 142644.

[6] R. A. Guidotti, F. W. Reinhardt, J. Odinek, *J. Power Sources* **2004**, *136*, 257.

[7] H. Guo, Z. H. Lv, Z. Y. Wu, B. Wei, *IET Electr. Power Appl.* **2013**, *7*, 214.

[8] C. P. Grey, J. M. Tarascon, *Nat. Mater.* **2017**, *16*, 45.

[9] E. S. Fan, L. Li, Z. P. Wang, J. Lin, Y. X. Huang, Y. Yao, R. J. Chen, F. Wu, *Chem. Rev.* **2020**, *120*, 7020.

[10] L. F. Han, Y. D. Hou, Y. J. Wang, X. B. Liu, J. Han, R. H. Xie, H. W. Mu, C. F. Fu, *Flow Meas. Instrum.* **2019**, *69*, 101622.

[11] A. Ghasemloonia, D. G. Rideout, S. D. Butt, *J. Pet. Sci. Eng.* **2015**, *131*, 150.

[12] C. Ke, X. Y. Song, *J. Dyn. Syst. Meas. Control-Trans. ASME* **2017**, *139*, 8.

[13] K. Kitada, E. Araki, T. Kimura, Y. Mizuguchi, M. Kyo, T. Saruhashi, I. Sawada, Y. Namba, M. Kinoshita, *IEEE J. Ocean. Eng.* **2013**, *38*, 158.

[14] R. Wada, T. Kaneko, M. Ozaki, T. Inoue, H. Senga, *Ocean Eng.* **2018**, *156*, 1.

[15] F. R. Fan, Z. Q. Tian, Z. L. Wang, *Nano Energy* **2012**, *1*, 328.

[16] M. Willatzen, Z. L. Wang, *Nano Energy* **2018**, *52*, 517.

[17] S. H. Pan, Z. N. Zhang, *Friction* **2019**, *7*, 2.

[18] G. Zhu, B. Peng, J. Chen, Q. S. Jing, Z. L. Wang, *Nano Energy* **2015**, *14*, 126.

[19] F. R. Fan, W. Tang, Z. L. Wang, *Adv. Mater.* **2016**, *28*, 4283.

[20] X. Guo, J. J. Shao, M. Willatzen, Y. Yang, Z. L. Wang, *Nano Energy* **2022**, *92*, 10.

[21] J. He, X. M. Fan, D. Y. Zhao, M. Cui, B. Han, X. J. Hou, X. J. Chou, *Sci. China-Inf. Sci.* **2022**, *65*, 9.

[22] M. Y. Xu, P. H. Wang, Y. C. Wang, S. L. Zhang, A. C. Wang, C. L. Zhang, Z. J. Wang, X. X. Pan, Z. L. Wang, *Adv. Energy Mater.* **2018**, *8*, 9.

[23] K. Wang, J. X. Zhou, H. J. Ouyang, Y. P. Chang, D. L. Xu, *Mech. Syst. Signal Pr.* **2021**, *151*, 15.

[24] A. N. Ravichandran, C. Calmes, J. R. Serres, M. Ramuz, S. Blayac, *Nano Energy* **2019**, *62*, 449.

[25] Y. Zhang, Q. X. Zeng, Y. Wu, J. Wu, S. L. Yuan, D. J. Tan, C. G. Hu, X. Wang, *Nano-Micro Lett.* **2020**, *12*, 11.

[26] Y. Wang, X. Y. Liu, T. Y. Chen, H. Wang, C. Q. Zhu, H. Y. Yu, L. G. Song, X. X. Pan, J. C. Mi, C. Lee, M. Y. Xu, *Nano Energy* **2021**, *90*, 10.

[27] B. Huang, P. Z. Wang, L. Wang, S. Yang, D. Z. Wu, *Nanotechnol. Rev.* **2020**, *9*, 716.

[28] J. Chen, Z. L. Wang, *Joule* **2017**, *1*, 480.

[29] T. L. Du, X. S. Zuo, F. Y. Dong, S. Q. Li, A. E. Mtui, Y. J. Zou, P. Zhang, J. H. Zhao, Y. W. Zhang, P. T. Sun, M. Y. Xu, *Micromachines* **2021**, *12*, 14.

[30] Q. H. Xu, Y. T. Lu, S. Y. Zhao, N. Hu, Y. W. Jiang, H. Li, Y. Wang, H. Q. Gao, Y. Li, M. Yuan, L. Chu, J. H. Li, Y. N. Xie, *Nano Energy* **2021**, *89*, 8.

[31] C. P. Vo, M. Shahriar, C. D. Le, K. K. Ahn, *Int. J. Pr. Eng. Man-Gt.* **2019**, *6*, 741.

[32] S. Chun, W. Son, H. Kim, S. K. Lim, C. Pang, C. Choi, *Nano Lett.* **2019**, *19*, 3305.

[33] S. Wang, Y. Wang, D. H. Liu, Z. Y. Zhang, W. X. Li, C. X. Liu, T. L. Du, X. Xiao, L. G. Song, H. C. Pang, M. Y. Xu, *Sensor Actuat. A-Phys.* **2021**, *317*, 112459.

[34] A. Uddin, G. S. Chung, *RSC Adv.* **2016**, *6*, 63030.

[35] C. Wu, H. Huang, S. Yang, G. J. Wen, *IEEE Sens. J.* **2020**, *20*, 13999.

[36] J. W. Lee, J. Jeong, D. Yoo, K. Lee, S. Lee, D. S. Kim, J. Y. Sim, W. Hwang, *Nano Energy* **2019**, *56*, 612.

[37] C. A. Wu, S. Yang, G. J. Wen, C. X. Fan, *Rev. Sci. Instrum.* **2021**, *92*, 9.

[38] S. M. Niu, Y. Liu, X. Y. Chen, S. H. Wang, Y. S. Zhou, L. Lin, Y. N. Xie, Z. L. Wang, *Nano Energy* **2015**, *12*, 760.

[39] L. Zhang, H. Wu, Y. Yu, X. H. Zeng, J. F. Zhou, B. Q. Xie, M. Shi, S. L. Huang, *7th International Conference on Fluid Mechanics*, Qingdao, PEOPLES R CHINA, **2015**.

[40] Y. A. Khulief, H. Al-Naser, *Finite Elem. Anal. Des.* **2005**, *41*, 1270.

[41] N. Al Batati, F. M. Hashim, W. Pao, *1st International Materials, Industrial, and Manufacturing Engineering Conference*, Johor Bahru, MALAYSIA, **2013**.

[42] J. Zare, S. J. Hashemi, G. Rashed, *Sci Res Essays* **2011**, *6*, 13.